Coordination Chemistry of Triphos-Fe(0) Ethylene Complexes and Their Application to CO_2 Valorization

Tristan T. Adamson, Katherine B. Uttley, Steven P. Kelley and Wesley H. Bernskoetter*

The Department of Chemistry, The University of Missouri, Columbia, Missouri, 65211, USA.

E-mail: bernskoetterwh@missouri.edu

Abstract

The coordination chemistry of zerovalent iron complexes bearing triphosphine ligands of the type $^{t}BuP(CH_2CH_2PR_2)_2$ (R = Et, ^{i}Pr, Cy) was attenuated via ancillary ligand effects. Iron(0) dinitrogen ethylene complexes, $[^{t}BuP(CH_2CH_2PR_2)]Fe(C_2H_4)(N_2)$ (R = Et, ^{i}Pr, Cy), were prepared via alkali metal reduction of the corresponding iron dichloride precursors and were characterized by single crystal X-ray diffraction. In complexes bearing ^{i}Pr and Cy substituted triphosphine ligands, reversible dissociation of dinitrogen from $[^{t}BuP(CH_2CH_2PR_2)]Fe(C_2H_4)(N_2)$ was observed, generating paramagnetic four coordinate iron(0) monoethylene species, $[^{t}BuP(CH_2CH_2PR_2)]Fe(C_2H_4)$ (R = ^{i}Pr, Cy). Conversely, the Et substituted $[^{t}BuP(CH_2CH_2PEt_2)]Fe(C_2H_4)(N_2)$ was stable in solution and reacted rapidly with additional ethylene to afford a five coordinate iron(0) bisethylene species, $[^{t}BuP(CH_2CH_2PEt_2)]Fe(C_2H_4)$. Analysis of structural parameters obtained from X-ray diffraction and IR stretching frequencies obtained from the iron dicarbonyl species, $[^{t}BuP(CH_2CH_2PR_2)]Fe(CO)_2$ (R = Et, ^{i}Pr, Cy) suggest the attenuations in coordination chemistry are likely steric in origin. Examination of CO_2 functionalization from $[^{t}BuP(CH_2CH_2PR_2)]Fe(C_2H_4)(N_2)$ (R = Et, ^{i}Pr, Cy) revealed selective formation of methylmalonic acid upon protonolysis of the insoluble organometallic product, consistent with the coupling of bound ethylene with two molecules of carbon dioxide.

Introduction

The relationship between the fundamental coordination chemistry of transition metal complexes and the associated influence on their reactivity has long been the foundation of organometallic reaction

development. In few places is this more evident than in transition metal mediated functionalization of small molecule substrates. The annals of metal-mediated small molecule activation are filled with examples where minor changes in the ancillary ligands bring profound changes to the chemo-, regio-, and stereoselectivity of such transformations.[1–5] A classic example is the difference in reactivity between the zirconocene dinitrogen (N_2) complexes $[(\eta^5\text{-}C_5Me_5)_2Zr(\eta^1\text{-}N_2)]_2(\mu_2,\eta^1,\eta^1\text{-}N_2)$[6] and $[(\eta^5\text{-}C_5Me_4H)_2Zr]_2(\mu_2,\eta^2,\eta^2\text{-}N_2)$ reported in 2004 where removal of one methyl substituent from C_5Me_5 enables N_2 hydrogenation.[2] Of course, just as often transition metal chemists spend considerable effort to alter an ancillary ligand only to achieve marginal attenuations of reactivity. Still, these endeavors to explore structure-reactivity relationships remain a cornerstone of small molecule activation chemistry. One small molecule of increasing significance is carbon dioxide (CO_2)- a renewable, abundant source of carbon. While many studies of CO_2 valorization focus on generating C_1 products via carbon monoxide (CO),[7–9] formate ($HCOO^-$),[10–13] or methanol (CH_3OH)[14–19] intermediates, the coupling of carbon dioxide with other small molecules such as ethylene (C_2H_4),[20–29] propylene (CH_3CHCH_2),[30,31] and acetylides[32–40] is an emerging alternative with the potential to produce more elaborate, high-value carboxylates.[41] In 1977, Hashimoto described a pioneering example of transition metal mediated CO_2-alkyne coupling using a phosphine-ligated Ni(0) species which functionalized CO_2 with 1-hexyne to produce a substituted pyrone, along with a mixture of other products.[33] This was shortly followed by Hoberg and coworkers who reported the first example of CO_2-olefin coupling using a nickel complex.[21] While many subsequent studies have investigated new nickel systems for CO_2-olefin coupling,[20,23,24,27,29] comparatively little work has been reported on iron or other more earth-abundant base metals. Iron is an attractive metal for the mediation of CO_2 valorization as it, like CO_2, is widely available, non-toxic, and inexpensive compared to nickel and other transition metals.

In the late 1980's, following a study in which an Fe(0) complex was found to mediate the coupling of CO_2 with butadiene,[42] Hoberg reported a rare example of iron-mediated CO_2-C_2H_4 coupling.[43] A simple Fe(0) source, $(Et_3P)_2Fe(C_2H_4)_2$, was found to produce methylmalonate or methyl succinate products in the presence of additional phosphine ligand (Figure 1).[43] The selectivity of the CO_2 functionalization was

strongly influenced by the nature of the added ligand, with PMe_3 affording the methyl ester of methylmalonic acid upon methanolysis of the organometallic product, whereas 1,2-bis(dicyclohexylphosphino)ethane (dcpe) yielded the methyl ester of succinic acid.[43] Curiously, in the absence of additional phosphine ligand, reaction of $(Et_3P)_2Fe(C_2H_4)_2$ with CO_2 produced only reductive disproportionation to carbonate (CO_3^{2-}) and CO complexes,[44] suggesting a delicate attenuation of the reaction pathways by the substituents and availability of exogenous phosphine ligands.[43] Unfortunately, there were few subsequent studies to elucidate the origins of these structure-reactivity differences or identify the precise Fe(0) species that promoted CO_2 activation.

After a decades long hiatus, recent studies on Fe(0)-mediated olefin and alkyne coupling have been reported. Recently, Field and coworkers described the coupling of CO_2 with various acetylides mediated by low valent iron dmpe (dmpe = 1,2-bis(dimethylphosphino)ethane) and depe (depe = 1,2-bis(diethylphosphino)ethane) complexes, in which unsaturated iron lactones were isolated and characterized (Figure 2).[39,40] While much of the reactivity of the depe and dmpe variants was analogous, important differences in the regioselectivity of the CO_2 coupling were observed with ancillary ligand changes. The dmpe iron complex coupled CO_2 and phenylacetylene to selectively produce an α-substituted unsaturated lactone,[40] while the more sterically hindered depe iron complex produced exclusively β-substituted lactones (Figure 2).[39] Using the depe chelate, our own laboratory has reported that $(depe)_2Fe(C_2H_4)$ produces an isolable 5-membered saturated metallalactone species via coupling of CO_2 and C_2H_4 (**A**; Figure 3).[28] Upon addition of a proton source, complex **A** liberates propionic acid.[28] Regrettably, the more economically desirable acrylate product resulting from β-H elimination of **A** could only be obtained in low yield with the addition of a strong base.[28] The inability of the iron-lactone **A** to form acrylate in good yield was partially attributed to its 18-electron configuration, which would necessitate a ligand dissociation event to enable β-H elimination.[28,45,46] Motivated by this limitation of **A**, as well as the literature precedent for attenuated reactivity in these systems via small changes to the ancillary ligands, we sought to investigate the coordination chemistry and CO_2 functionalization potential of low-valent iron triphosphine complexes. Herein we describe the synthesis of a series of (Triphos)Fe(0) ethylene complexes

(Triphos = ^{t}BuP($CH_2CH_2PR_2$)$_2$ (R = Et, ^{i}Pr, Cy)).[47,48,49] These species were characterized by a combination of NMR and IR spectroscopy as well as X-ray diffraction analysis. Several differences in their coordination chemistry were observed, including the reversible binding of unsaturated ligands such as C_2H_4 and N_2. Each of the (Triphos)Fe(0) ethylene complexes mediate CO_2 functionalization to produce methylmalonic acid in good yield with high selectivity.

Figures for Introduction:

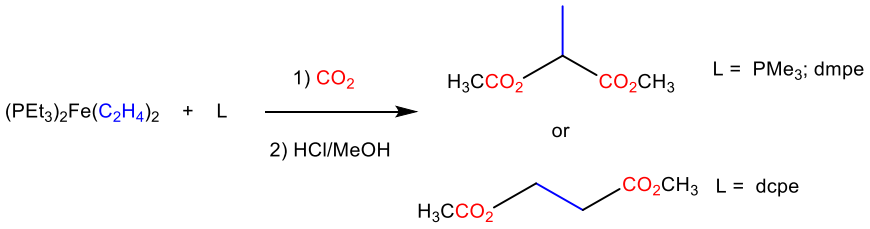

Figure 1: CO_2-C_2H_4 coupling mediated by $(Et_3P)_2Fe(C_2H_4)_2$ reported by Hoberg and coworkers.[43]

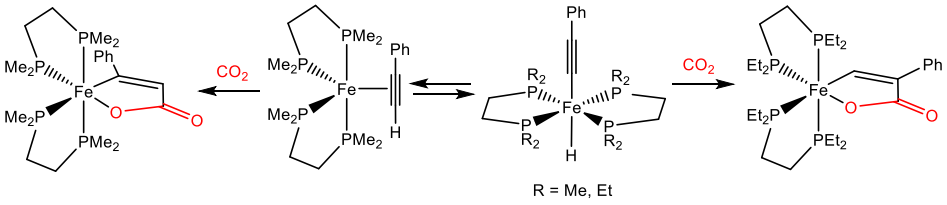

Figure 2: Fe(0) mediated coupling of CO_2 with phenylacetylene reported by Field and coworkers.[39,40]

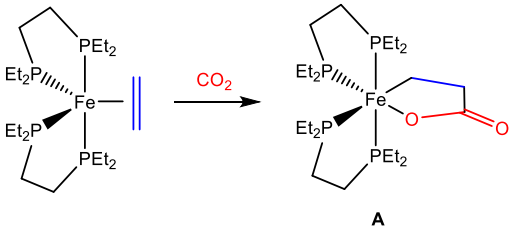

Figure 3: CO_2-C_2H_4 coupling mediated by $(depe)_2Fe(C_2H_4)$.[28]

Results and Discussion

Synthesis and Characterization of (Triphos)Fe(0) Ethylene Complexes

Preparation of the (Triphos)Fe complexes began by metalation of three variants of ^{t}BuP($CH_2CH_2PR_2$)$_2$ with $FeCl_2$ affording the five-coordinate species [^{t}BuP($CH_2CH_2PR_2$)$_2$]$FeCl_2$ (R = Et (**1a**), ^{i}Pr (**1b**), Cy (**1c**)[49]) in good yields (Figure 4). The dichloride complexes are all paramagnetic, with solution magnetic moments ranging from 5.0 – 5.5 μ_B measured by solution Evan's method as expected for a high spin Fe(II) center.[50] Despite their paramagnetism, complexes **1a-c** featured broad, observable ^{1}H NMR signals with chemical shifts from -4 ppm to 114 ppm that provided convenient signatures for their presence in solution.

Metal mediated CO_2-C_2H_4 coupling reactions have most commonly been reported with zerovalent metal centers,[20,21,23,25,27,28,43,51–56] though Chirik and coworkers have described an interesting Fe(II) example containing a redox-active pyridine diimine ligand.[57] Given the prevalence of low valent metal promotors, we sought to study the synthesis and coordination chemistry of (Triphos)Fe(0) ethylene complexes, which were targeted via potassium graphite (KC_8)[58] reduction of the corresponding dihalide (Figure 5). Initial efforts examined reduction of the PEt_2 variant **1a**, as it offers the closest steric comparison to the previously studied complexes (depe)$_2$Fe(C_2H_4) and (Et_3P)$_2$Fe(C_2H_4)$_2$. KC_8 reduction of **1a** in THF under *ca* 1.5 atm of C_2H_4 and subsequent exposure to a N_2 atmosphere afforded [^{t}BuP($CH_2CH_2PEt_2$)$_2$]Fe(C_2H_4)(N_2) (**2a**) as a red-orange solid. The ^{31}P NMR spectrum of **2a** in C_6D_6 exhibited triplet and doublet resonances at δ 124.07 and 85.83 ppm respectively, suggesting formation of a product in which the two PEt_2 sites are equivalent. The resonance for the bound C_2H_4 was found at δ 24.1 ppm in the ^{13}C NMR spectrum, which correlated to a broad ^{1}H resonance at δ 1.53 ppm in the ^{1}H-^{13}C HSQC NMR spectrum. The presence of the N_2 ligand in pentane solution was confirmed by an intense IR absorbance at 2050 cm^{-1}, which is near the frequency reported for the related (Triphos)Fe (bis)dinitrogen complexes.[49]

Cooling a concentrated pentane solution of **2a** to -35 °C under a N_2 atmosphere produced crystals suitable for X-ray diffraction analysis (Figure 6). The molecular structure exhibits a distorted trigonal bipyramidal ($\tau = 0.79$)[59,60] coordination environment about the iron including a *fac* oriented Triphos chelate, an equatorial C_2H_4 ligand and an axial N_2 ligand. The elongated 1.410(4) Å C(1)-C(1a) bond distance for the coordinated C_2H_4 ligand of **2a** suggests considerable reduction of the olefin, though this value is intermediate of the analogous distances in $(PEt_3)_2Fe(C_2H_4)_2$ (1.382(4) Å)[43] and $(depe)_2Fe(C_2H_4)$ (1.432(2) Å).[28] The relative reduction of the bound C_2H_4 in these similar species is likely a consequence of the varied number of coordinated phosphine ligands in each complex. The 1.115(3) Å N(1)-N(2) distance is little changed from that of free N_2, suggesting minimal reduction of the axial ligand.[49] Addition of one equivalent of C_2H_4 to a C_6D_6 solution of **2a** resulted in *ca* 35% conversion to a new species over a period of 3 days. The ^{31}P NMR spectrum of the mixture exhibited new triplet and doublet resonances at δ 156.74 and 74.84 ppm, respectively. The presence of free C_2H_4 in the ^1H NMR spectrum along with the absence of additional conversion suggests a ligand substitution equilibrium between **2a** and a (Triphos)Fe (bis)ethylene species, $[^tBuP(CH_2CH_2PEt_2)_2]Fe(C_2H_4)_2$ (**4a**) (Figure 5). Unfortunately, complete substitution of N_2 proved difficult reaching only *ca* 85% conversion to **4a** under 2 atm of C_2H_4 after 3 days. Immediate reversion to **2a** upon removal of the excess C_2H_4 and exposure to N_2 obviated isolation of **4a**. The identity of **4a** was confirmed by the addition of $^{13}C_2H_4$ to a sample of **2a**, which resulted in the appearance of two broad signals at δ 29.4 (m) and 24.7 (s) ppm in the ^{13}C NMR spectrum, as well as enhancement of the signal for the bound C_2H_4 in residual **2a** (Figure S27). The complex splitting for the downfield resonance of **4a** is likely due to incompletely resolved ^{31}P-^{13}C and ^{13}C-^{13}C coupling. These factors along with possible exchange with free $^{13}C_2H_4$ likely contribute to the broadness of both resonances.

Alkali metal reductions were also performed using the P^iPr_2 and PCy_2 substituted variants **1b** and **1c** yielding crystalline samples of Fe(0) species analogous to **2a,** $[^tBuP(CH_2CH_2PR_2)_2]Fe(C_2H_4)(N_2)$ (R = ^{i}Pr (**2b**) and Cy (**2c**)) (Figure 5). The solid-state structures of **2b** and **2c** (Figure 6) exhibited slightly distorted trigonal bipyramidal geometries, with τ values of 0.96 and 0.93 respectively. The C-C bond lengths of the coordinated C_2H_4 ligands range from 1.402(4) (**2c**) to 1.418(6) (**2b**) indicating a similar

degree of reduction among the series of (Triphos)Fe ethylene complexes. There is no statistically significant difference in the N-N bond lengths of the coordinated N_2 ligands in the series of complexes. As with **2a**, IR spectra of **2b** and **2c** collected in pentane confirmed at least partial retention of the N_2 ligand in solution (*vide infra*). However, addition of 1 atm of C_2H_4 to **2b** and **2c** did not result in formation of (Triphos)Fe (bis)ethylene species as judged by ^{1}H and ^{31}P NMR spectroscopy, even after prolonged heating at 50 °C. In further contrast to **2a**, solution NMR spectra of dissolved crystalline samples of **2b** and **2c** exhibited a set of broad resonances at unusually high and low field chemical shifts, in addition to the set of sharp resonances consistent with the molecular structures obtained by X-ray diffraction. Analysis of multiple crystalline samples of **2b** and **2c** found no evidence of a second structure or impurity for either in the solid state. These observations suggest that both **2b** and **2c** are in equilibrium with a paramagnetic species in solution. Additionally, analysis of ^{1}H NMR spectra collected after removal of the N_2 atmosphere revealed an increase in the amount of paramagnetic material relative to the signals for **2b** or **2c**. Renewed exposure to a N_2 atmosphere restored the original integration ratios between the resonances for **2b** or **2c** and the paramagnetic species. Similar reversible shifts in the equilibrium mixture were observed upon heating **2b** and **2c**. Based on these observations, and the precedent for paramagnetic, tetrahedral, 16-electron Fe(0) complexes,[61–63] the paramagnetic material in each equilibrium are tentatively assigned as the four-coordinate Fe(0) ethylene complexes [^{t}BuP($CH_2CH_2PR_2$)$_2$]Fe(C_2H_4) (R = ^{i}Pr (**3b**), Cy (**3c**)) produced by dissociation of the N_2 ligand from **2b** and **2c** (Figure 5).

The equilibrium between complexes **2** and **3** in solution obviated isolation of pure **3b** or **3c**, and their paramagnetism limited the use of NMR spectroscopy in structural assignment. Therefore, we attempted to derivatize **3b** and **3c** by reaction with CO and dihydrogen (H_2) to further support the proposed structures (Figure 7). Treatment of a benzene solution of the **2b**/**3b** equilibrium mixture with an atmosphere of H_2 produced an immediate color change from orange to dark red. ^{1}H NMR spectroscopy revealed the presence of free ethane, identified by a singlet resonance at δ 0.80, presumably formed from hydrogenation of the bound C_2H_4 on **2b** and **3b**, as well as a large singlet at 4.85 ppm that integrates for 6 protons. A set of three equal integration resonances at δ 110.8 (d), 109.6 (dd), and 9.9 (d) ppm was observed in the ^{31}P

NMR spectrum. The significant upfield chemical shift of one ^{31}P resonance suggests κ^2-coordination of the Triphos ligand.[64] No additional signals for a paramagnetic species were detected. These data are consistent with formation of an electronically saturated, partially chelated, η^6-benzene adduct, [κ^2-^{t}BuP($CH_2CH_2P^iPr_2$)$_2$]Fe(η^6-C_6H_6) (**5b**) (Figure 7), which has closely related congeners with similar NMR spectral features.[65] The formation of only one compound with no evidence of any anionic ligands on **5b** is in agreement with the assignment of the paramagnetic compound as **3b**, and supports our hypothesis that **2b** and **3b** are in equilibrium as they both converge to one structure upon reaction of H_2. This is further supported by treatment of equilibrium solutions of **2b**/**3b** and **2c**/**3c** with 1 atm of CO (Figure 7). At ambient temperature, full conversion to the (Triphos)Fe dicarbonyl complexes **6b** and **6c** was observed within 30 minutes, identified by comparison of the ^{31}P NMR spectra with authentic samples produced by KC_8 reduction of **1b** and **1c** under a CO atmosphere.[66] The P^iPr_2 variant **6b** was also characterized by X-ray diffraction (Figure 8). Notably, treatment of **2a** with 1 atm of CO only led to *ca* 5% conversion to the dicarbonyl **6a** after 30 minutes, and only 35% conversion after 2 weeks at ambient temperature, consistent with the reduced lability of the dinitrogen ligand in **2a** relative to **2b** and **2c**.

The observed reactivity with CO and H_2 is consistent with the proposed structures for the equilibrium mixture of complexes **2** and **3**. Examination of various metrical parameters for complexes **2a-c** suggests all three species are electronically similar. This is supported by the solid-state N≡N stretching frequencies of **2a-c** which only differ by a total of 15 cm^{-1} and is further confirmed by infrared analysis of the corresponding iron dicarbonyl species **6a-c**, which reveals the average C≡O stretching frequencies span a range of only 7 cm^{-1} (Table S1). Together, these data indicate that the ability of **2a** to bind an additional C_2H_4 to form **4a** is largely a steric phenomenon. By comparison, **2b** and **2c** appear incapable of adding even the small C_2H_4 molecule as a fifth ligand, and in solution alleviate steric hindrance by extrusion of N_2 to form an equilibrium with the four coordinate species **3b** and **3c.** To illustrate the differences in sterics among **2a-c**, percent buried volume ($\%V_{Bur}$)[67] calculations were performed and the results depicted in Table 1. As expected, calculations show that **2a** has a lower $\%V_{Bur}$ than either **2b** or **2c**. More specific to the observed ligand substitution chemistry, **2a** also has the lowest $\%V_{Bur}$ in the N_2-containing quadrant (the SW

quadrant as depicted in the Table 1 orientation) at 31.1%, while **2b** and **2c** exhibit higher steric hinderance in this area with $\%V_{Bur}$ = 36.7% and 35.2% respectively. Overall, this collection of data and observations strongly suggest any differences in coordination chemistry between the PEt_2 and P^iPr_2/PCy_2 (Triphos)Fe(0) variations is controlled by steric attenuation of the ancillary ligand.

Reactivity with Carbon Dioxide

Preparation of the series of (Triphos)Fe ethylene dinitrogen complexes **2a-c** provided an opportunity to investigate attenuating effects the Triphos ligand, and its steric variations, brings to Fe(0) mediated CO_2-C_2H_4 coupling reactions. Initial CO_2 functionalization experiments were conducted in the presence of excess C_2H_4 to limit deleterious reductive disproportionation reactions which may arise from CO_2 for C_2H_4 ligand substitution.[28,44,68] Addition of 6 eq of C_2H_4 and 2 eq of $^{13}CO_2$ to a C_6D_6 solution of **2a** resulted in the formation of a dark red precipitate within 15 minutes at ambient temperature. After 18 hours, nearly all organometallic material had converted to the insoluble species as evidenced by a loss of all relevant signals in the ^{31}P NMR spectrum.

The isotopically labelled dark red precipitate proved essentially insoluble in most solvents examined by our laboratory, including hexamethyldisiloxane, pentane, diethyl ether, benzene, toluene, THF, dichloromethane, chloroform, chlorobenzene, acetone, ethanol, dimethylacetamide, and DMSO. While the isolated precipitate did slightly color acetonitrile solutions to a light pink, no NMR signals were observed for these solutions even after prolonged acquisitions, indicating a very low concentration of the species and precluding definitive structural assignment via NMR spectroscopy.

In an effort to further characterize the product of CO_2 functionalization, an acetonitrile suspension of the dark red precipitate was treated with 10 eq of anhydrous hydrogen chloride, resulting in rapid bleaching and dissolution of the mixture to afford a light-yellow solution. The ^{13}C NMR spectrum of the protonolysis samples derived from $^{13}CO_2$ exhibit a single enhanced resonance at 171.6 ppm (Figure S28). Comparison to authentic samples and ^1H-^{13}C HMBC NMR analysis identified this organic product as methylmalonic acid (MMA), resulting from the coupling of C_2H_4 in **2a** with two $^{13}CO_2$ molecules (Figure 9). Allowing solutions of **2a** to equilibrate with **4a** under an ethylene atmosphere for 24 hours prior to $^{13}CO_2$

addition produced identical results, suggesting insertion of multiple ethylene molecules is not competitive with the two CO_2 coupling reactions. The MMA yield per iron was found to be 76.3%, based on quantitative ^{13}C NMR spectroscopy (Table S2). This yield suggests that the resulting MMA complex is likely composed of a 1:1 MMA to Fe ratio.

The functionalization of CO_2 by **2a** was further confirmed by solid state IR spectroscopy of samples generated using $^{13}CO_2$ and unlabeled CO_2. The IR spectrum of the unlabeled functionalization product exhibited asymmetric stretches at 1630 and 1585 cm^{-1} and symmetric stretches at 1379 and 1278 cm^{-1} for an Fe bound MMA fragment (Figure S29). The significant difference in frequency between the asymmetric and symmetric stretches is consistent with κ^1-coordination of the MMA fragment.[69] Use of $^{13}CO_2$ shifted those bands to 1597 (a), 1546 (a), 1368 (s), and 1270 (s) cm^{-1} respectively (Figure S30). These shifts are significantly smaller than that predicted by the Hooke's law model, but agree well with previous reports of κ^1-carboxylates coordinated to iron.[70] The relatively small change in frequencies suggests that the carboxylate vibrational stretching modes are strongly coupled to additional modes not directly involving the carboxylate atoms.[70] While a more definitive structural assignment product cannot be made with the data in hand, we tentatively propose the monometallic structure **B** as the likely product of CO_2 functionalization by **2a** (Figure 10). Iwasawa and coworkers recently have characterized a nickel-MMA complex analogous to **B** by X-ray diffraction with closely related IR spectral features.[29]

Based on our experimental observations and prior studies of CO_2-olefin/alkyne coupling, one plausible mechanism for the reaction of **2a** with CO_2 is illustrated in Figure 10. Initial reaction of **2a** and CO_2 likely produces an iron γ-lactone complex, analogous to species **A** observed from $(depe)_2Fe(C_2H_4)$ (Figure 3).[28] The selective formation of MMA from protonolysis experiments (Figure 9) indicates that the 5-membered ring undergoes contraction to the iron β-lactone isomer. Analogous γ- to β-metallalactone isomerization has been directly observed in nickel promoted CO_2-C_2H_4 coupling and likely occurs via a sequence of β-hydride elimination followed by 2,1-insertion of a transient acrylate ligand.[29,71] Subsequent insertion of a second CO_2 in the Fe-C bond would afford the proposed (Triphos)Fe dicarboxylate **B**, similar to recently reported methyl malonate structures on nickel. Related CO_2 insertions into iron-alkyl groups to

Commented [BWH1]: Insert ref 29

have been been reported using iron-bis(diphosphine)complexes.[72] Alternatively, CO_2 functionalization could occur via transient formation of an iron vinyl species and two carbenoid-like insertions of CO_2 at the β-carbon, in analogy to recent proposals for iron-acetylene based CO_2 functionalization.

Commented [BWH2]: Insert ref to field paper

The selective formation of an iron-MMA complex mirrors the reactivity reported by Hoberg when using small ancillary ligands such as PMe_3 (Figure 1).[43] However, the origin of the selectivity toward MMA compared to other possible protonation products such as acrylic acid, propionic acid, or succinic acid is not self-evident. Clearly the insertion of the second CO_2 molecule is competitive with or faster than the first CO_2 coupling as iron lactone species are not observed by *in situ* NMR spectroscopy and no propionic acid is detected in the protonolysis experiments. Additionally, treatment of **2a** with only 1 eq of CO_2 affords partial conversion to **B** leaving approximately 50% of residual **2a** in solution. Recently, an investigation into photoredox catalyzed formation of methylmalonate from CO_2/C_2H_4 coupling at nickel(0) revealed that CO_2 insertion into a nickel lactone occurred after a relatively slow isomerization from the 5-membered to 4-membered metallacycle, suggesting that the γ-lactone species may be reticent to insert a second CO_2 molecule.[29] In the case of **2a**, the selectivity for MMA could also originate from a faster rate for γ- to β-metallalactone isomerization compared to the rate of the second CO_2 insertion. Unfortunately, the concurrent precipitation of the (Triphos)Fe dicarboxylate has obviated a more detailed study of these pathways.

Hoberg's prior observation of a strong ancillary ligand dependence in the reactivity of $(Et_3P)_2Fe(C_2H_4)_2$ motivated experiments to assess the effect of exogenous ligands on **2a**-promoted CO_2 functionalization.[43] However, addition of 1.2 equivalents of pyridine, PCy_3, PPh_3, and $PMePh_2$, PMe_2Ph and PMe_3 to **2a** prior to CO_2 activation had no influence on the selectivity of the coupling reaction, giving MMA as the sole product. In fact, ^{31}P NMR analysis of the samples prior to CO_2 addition suggests that **2a** is too sterically encumbered to even coordinate all but the smallest exogenous ligands, PMe_2Ph and PMe_3 (Figure S31-S32). Likewise, we attempted to alter the selectivity of CO_2 functionalization via attenuation of the Triphos ligand substituents employing **2b** and **2c**. However, the increased steric hindrance of **2b** and **2c** did not improve the solubility of the iron CO_2 functionalization product or significantly influence the

product distribution. Only trace propionic acid was detected from protonolysis experiments along with yields of MMA comparable to those obtained with **2a** (Figure 9). Additionally, performing CO_2-C_2H_4 coupling reactions in the presence of potassium *tert*-butoxide to trap the intermediate iron lactones did not afford detectable acrylate formation from **2a**. Thus, the selectivity of CO_2-C_2H_4 coupling by (Triphos)Fe complexes strongly favors MMA formation and cannot be easily altered by steric attenuation of the ancillary ligand. While the insolubility of the (Triphos)Fe MMA complexes obviated efforts to explore catalytic applications of this reaction, the rapid rate of the second CO_2 insertion and the high selectivity for MMA suggests that related iron species could be promising targets for new CO_2 valorization studies.

Concluding Remarks

The series of Triphos iron(0) ethylene dinitrogen complexes, [^{t}BuP($CH_2CH_2PR_2$)$_2$]Fe(C_2H_4)(N_2) (R = Et, ^{i}Pr, Cy), have been isolated and crystallographically characterized. Significant differences in the coordination chemistry of these complexes was observed, including the reversible binding of the dinitrogen ligand which leads to the formation of paramagnetic four-coordinate Triphos iron(0) ethylene complexes for the larger P^{i}Pr$_2$ and PCy$_2$ substituted variants. In the case of the smaller PEt$_2$ substituted species, addition of ethylene promotes dinitrogen substitution to afford a Triphos iron(0) bis(ethylene) complex. All three Triphos iron(0) ethylene dinitrogen complexes mediate CO_2-C_2H_4 coupling to produce MMA complexes with high selectivity; however, the insolubility of the iron-MMA species limited efforts to investigate the mechanism of CO_2 functionalization. Comparison of these results with prior studies of CO_2-C_2H_4 coupling using (depe)$_2$Fe(C_2H_4) and (Et_3P)$_2$Fe(C_2H_4)$_2$ suggests that coordinately unsaturated iron lactone complexes, or similar complexes bearing monodentate ligands that can easily create open coordination sites, are highly selective for the functionalization of two molecules of CO_2 per C_2H_4 unit and may be excellent targets for the production of methylmalonate or succinate products.[28,43] In contrast, 18-electron iron lactone complexes appear to resist coupling of a second CO_2 molecule and may be promising targets for the production of acrylate or propionate products, provided issues of product release from the metal can be suitably addressed. Interestingly, the relative reactivity of CO_2-C_2H_4 coupling at iron(0) appears distinct to those observed for nickel analogues where 16-electron nickel lactone species seldom couple two molecules of CO_2 per C_2H_4

unit,[20,23,24,27,71] instead offering isolable metallocycles or undergoing β-hydride elimination reactions. These observations suggest a critical role for the *d*-electron configuration in controlling the CO_2-C_2H_4 coupling pathways for these otherwise similar systems. While attenuation of the ancillary ligand sterics can alter the coordination chemistry of the iron(0) species, it appears that changes to the electronic environment may be more productive in manipulating the CO_2-C_2H_4 coupling selectivity. Efforts to better elucidate these influences on the transition metal promoted CO_2 reductive coupling reaction are continuing in our laboratory.

Figures for Results Section:

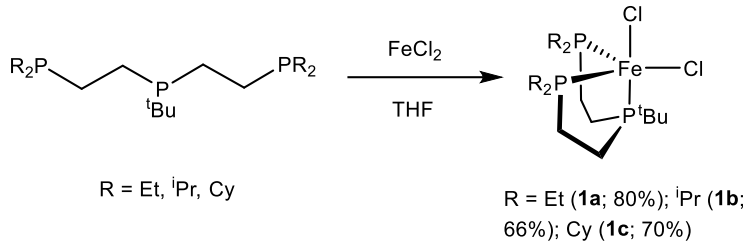

Figure 4: Synthesis of the dichloride complexes **1a-c**.

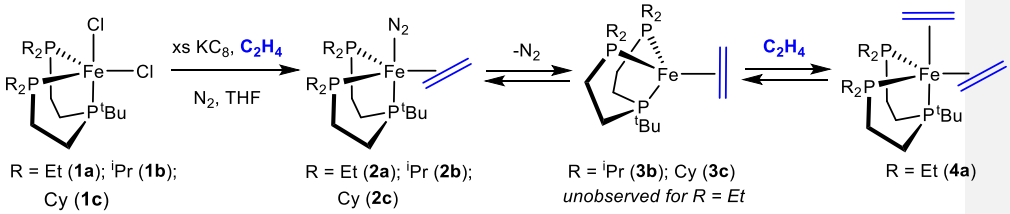

Figure 5: Synthesis and coordination chemistry of (Triphos)Fe complexes.

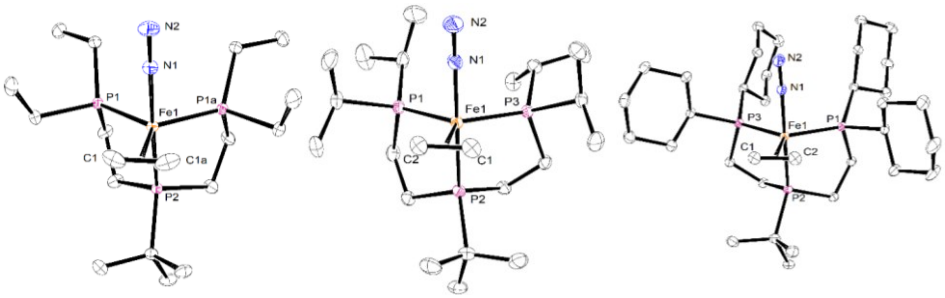

Figure 6: Molecular structures of **2a** (left), **2b** (center) and **2c** (right) at 30% ellipsoids. All hydrogen atoms have been removed for clarity. Structures **2b** and **2c** contain two independent molecules in the asymmetric unit cell. Only one molecule is shown for each.

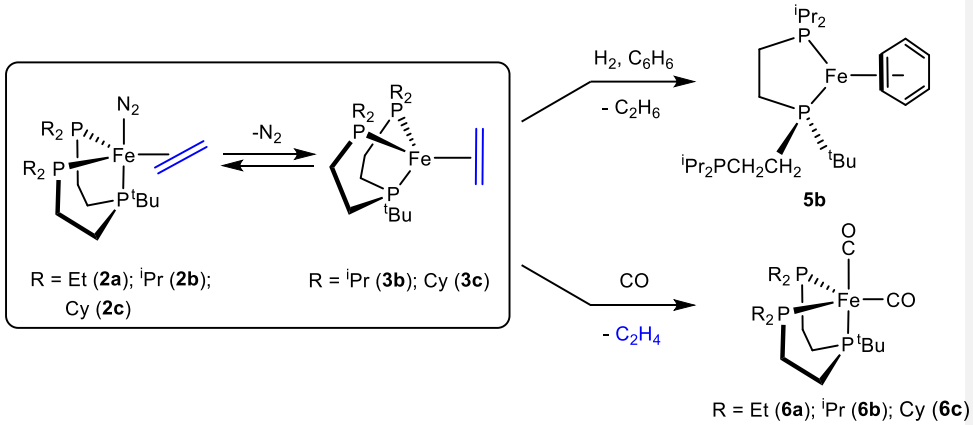

Figure 7: Reaction of complexes **2** and **3** with dihydrogen and carbon monoxide.

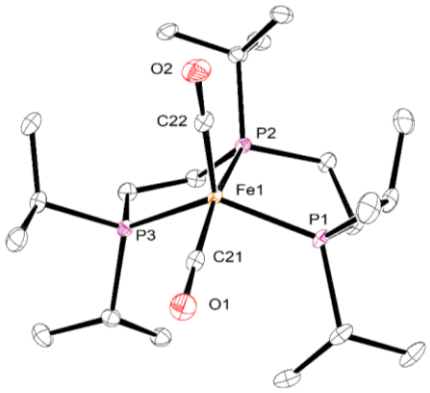

Figure 8: Molecular structure of **6b** at 30% ellipsoids. All hydrogen atoms have been removed for clarity. Two molecules were observed in the asymmetric unit. Selected metrical parameters for the depicted molecule: C(21)-O(1): 1.164(2) Å, C(22)-O(2): 1.165(2), Fe(1)-C(21): 1.7493(16), Fe(1)-C(22): 1.7577(16).

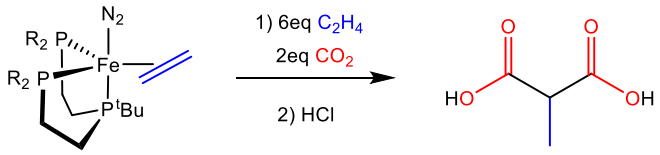

R = Et (**2a**); ^{i}Pr (**2b**); Cy (**2c**)

2a; Yield 76%
2b; Yield 81%
2c; Yield 88%

Figure 9: The reaction of **2a-c** with CO_2 followed by protonolysis to yield methylmalonic acid (MMA).

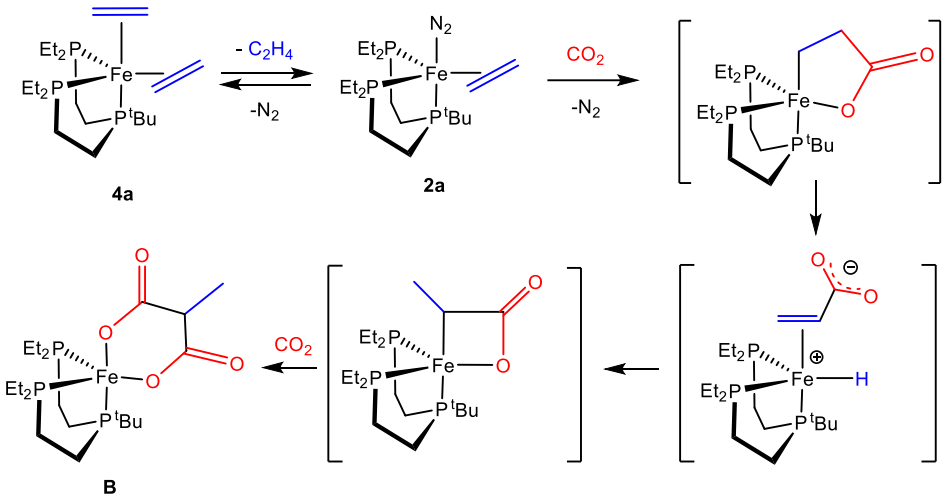

Figure 10: Proposed mechanism for the generation of the iron-MMA complex **B** from the reaction of **2a-c** with CO_2.

Table 1: Percent buried volume ($\%V_{Bur}$) descriptions for complexes 2a-c.

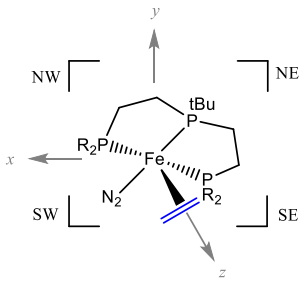

Quadrant	$\%V_{Bur}$ [a]		
	2a	**2b**	**2c**
SW	31.1	36.7	35.2
NW	69.7	74.8	76.2
NE	86.2	88.0	88.2
SE	72.1	76.3	76.5
Total	64.8	68.9	68.4

[a] Calculated using SambVca 2.1.[67]

Experimental Section

General Experimental Procedures. All work was performed using standard air-free vacuum, Schlenk, cannula, and glovebox techniques. All chemicals were purchased from Aldrich, Alfa Aesar, Fischer, Strem, or VWR; isotopically enriched reagents were purchased from Cambridge Isotope Laboratories. ^{t}BuP(CH$_2$CH$_2$PR$_2$)$_2$ (R = Et, Cy),[47–49] [^{t}BuP(CH$_2$CH$_2$PCy$_2$)$_2$]FeCl$_2$[49] and KC$_8$[58] were synthesized according to the literature procedure by Mézailles et al;[48] ^{t}BuP(CH$_2$CH$_2$P^{i}Pr$_2$)$_2$ was synthesized according to the procedure for the analogous Et and Cy derivatives using diisopropyl phosphine. Phenoxide bases were prepared by reaction of sodium hydride with the corresponding phenol derivative.[27] Solvents were dried and degassed according to literature procedures.[73] 99.8% carbon dioxide, and dry ethylene were used as received from Airgas. NMR spectra were recorded on Bruker 300 MHz DRX, 500 MHz DRX, or 600 MHz spectrometers. ^{1}H and ^{13}C NMR spectra were referenced to solvent signals,[74] while ^{31}P NMR spectra were referenced to an 85% phosphoric acid external standard. Sample purity for air-sensitive compounds where elemental analysis was unsuccessful was confirmed via NMR spectroscopy. X-ray crystallographic data were collected on a Bruker SMART CCD system. Samples were collected in inert oil and quickly transferred to a cold gas stream. The structures were solved from direct methods and Fourier syntheses and refined by full-matrix least-squares procedures with anisotropic thermal parameters for all non-hydrogen atoms.

Synthesis of [^{t}BuP(CH$_2$CH$_2$PEt$_2$)$_2$]FeCl$_2$ (1a). A 20 mL scintillation vial was charged with 56 mg (0.44 mmol) FeCl$_2$ and 156 mg (0.48 mmol) ^{t}BuP(CH$_2$CH$_2$PEt$_2$)$_2$ and approximately 7 mL of THF. The reaction was stirred overnight at ambient temperature before filtering the solution through Celite and concentration under vacuum. Layering of the concentrated THF solution with pentane at -35 °C yielded 158 mg (79.6 yield) of **1a** as dark blue crystals. Anal. found (calcd) for C$_{16}$H$_{37}$P$_3$FeCl$_2$: C, 43.30 (42.79); H, 7.77 (8.30). ^{1}H NMR (300 MHz, C$_6$D$_6$): δ 98.24 ($\upsilon_{1/2}$ = 6573.9 Hz) 91.38 ($\upsilon_{1/2}$ = 1651.0 Hz), 69.33 ($\upsilon_{1/2}$ = 2551.5 Hz), 60.60 ($\upsilon_{1/2}$ = 2191.3 Hz), 9.10 ($\upsilon_{1/2}$ = 450.3 Hz), the following signals were not suitably resolved to determine the peak width at half max: 4.31 (br s), 3.90 (br s), 3.06 (br s), 2.86 (br s), 2.62 (br s), 1.68 (br s), 1.50 (br s). μ_{eff} (Evans, THF-d_8, 298K) = 5.5 μ_B.

Synthesis of [^{t}BuP(CH$_2$CH$_2$P^{i}Pr$_2$)$_2$]FeCl$_2$ (1b). This complex prepared in a procedure analogous to that described for **1a**, using 85 mg (0.67 mmol) $FeCl_2$ and 278 mg (0.73 mmol) ^{t}BuP(CH$_2$CH$_2$P^{i}Pr$_2$)$_2$ to obtain **1b** as a THF soluble maroon oil. Precipitation via addition of pentane and drying in vacuo produced 221 mg of an off-white foam (65.6% yield). The complex was used in subsequent reactions without additional purification. ^{1}H NMR (600 MHz, C_6D_6): δ 9.31 ($\upsilon_{1/2}$ = 542.0 Hz), 6.45 ($\upsilon_{1/2}$ = 86.2 Hz). μ_{eff} (Evans, THF-d_8, 298K) = 5.0 μ_B.

Synthesis of [^{t}BuP(CH$_2$CH$_2$PEt$_2$)$_2$]Fe(C$_2$H$_4$)(N$_2$) (2a). A 100 mL heavy walled glass reaction vessel was charged with 500 mg (1.1 mmol) of **1a** and 451 mg (3.3 mmol) KC_8 inside a nitrogen filled glovebox. On a vacuum line approximately 20mL of THF and 5.6 mmol $C_2H_{4(g)}$ were condensed into the vessel at -196 °C. The reaction vessel was allowed to warm to ambient temperature and stirred overnight. The volatiles were then removed in vacuo, and the residue extracted with pentane inside a nitrogen glovebox. The filtrate was slightly concentrated before recrystallizing at -35 °C overnight. Reddish-orange crystals of **2a** were isolated in 78% yield (376 mg). Multiple NMR peaks could not be definitively assigned due to significant overlap of ligand signals. ^{1}H NMR (600 MHz, C_6D_6): δ 2.22 – 1.79 (m, 8H), 1.66 – 1.39 (m, 2H), 1.53 (m, 4H, Fe-C$_2$*H*$_4$), 1.35 – 1.20 (m, 7H), 1.20 – 1.00 (m, 8H), 1.00 – 0.81 (m, 3H), 0.71 (d, 9H, *J* = 10.9 Hz, P-^{t}BuC*H*$_3$).^{13}C {^{1}H} NMR (600 MHz, C_6D_6): δ 27.7 (d, *J* = 2.5 Hz), 25.3 – 24.8 (m), 24.1 (d, *J* = 4.0 Hz, H$_2$*C*=*C*H$_2$), 23.5 (t, *J* = 5.8 Hz), 9.3 (d, *J* = 37.5 Hz), 8.9 (s), 8.8 (s), two resonances assumed to correspond to coincident carbons. ^{31}P {^{1}H} NMR (300 MHz, C_6D_6): δ 124.07 (t, 1P, *J* = 36.7 Hz), 85.83 (d, 2P, *J* = 36.5 Hz). IR (KBr): $\upsilon_{N\equiv N}$ = 2043 cm^{-1}. IR (C_5H_{12}): $\upsilon_{N\equiv N}$ = 2050 cm^{-1}.

Synthesis of [^{t}BuP(CH$_2$CH$_2$P^{i}Pr$_2$)$_2$]Fe(C$_2$H$_4$)(N$_2$) (2b). This complex was prepared in a procedure analogous to that described for **2a**, using 355 mg (0.70 mmol) of **1b,** 368 mg (2.1 mmol) KC_8, and 4.2 mmol $C_2H_{4(g)}$ to obtain 218 mg (63.2% yield) of **2b** as a reddish-orange crystalline solid. Multiple NMR peaks could not be definitively assigned due to significant overlap of ligand signals. ^{1}H NMR (600 MHz,

C_6D_6): δ 2.64 – 2.53 (m, 2H), 2.35 (br s, 2H), 2.29 – 2.19 (m, 2H), 1.65 – 1.53 (m, 2H), 1.53 – 1.45 (m, 2H), 1.42 – 1.33 (m, 12H), 1.30 – 1.13 (m, 15H), 1.07 – 0.96 (m, 3H), 0.73 (d, 9H, J = 10.4 Hz, P-^{t}BuCH_3). ^{13}C {^{1}H} NMR (600 MHz, C_6D_6): δ 35.2 (d, J = 6.9 Hz), 33.7 – 33.5 (m), 33.1 (t, J = 10.0 Hz), 28.1 (s), 26.0 (dt, J = 13.2, 20.1 Hz), 25.2 (dt, J = 5.8, 13.5 Hz), 24.9 (d, J = 4.5 Hz), 20.5 (d, J = 42.7 Hz), 20.2 (d, J = 5.4 Hz). ^{31}P {^{1}H} NMR (300 MHz, C_6D_6): δ 120.92 (t, 1P, J = 26.4 Hz), 96.49 (d, 2P, J = 26.3 Hz). IR (KBr): $\upsilon_{N\equiv N}$ = 2028 cm^{-1}. IR (C_5H_{12}): $\upsilon_{N\equiv N}$ = 2058 cm^{-1}.

Synthesis of [^{t}BuP($CH_2CH_2PCy_2$)$_2$]Fe(C_2H_4)(N_2) (2c). This complex was prepared in a procedure analogous to that described for **2a**, using 320 mg (0.48 mmol) of **1c**, 169 mg (1.3 mmol) KC_8, and 2.9 mmol $C_2H_{4(g)}$ to obtain 178 mg (56.9% yield) of **2c** as a dark orange crystalline solid. Multiple NMR peaks could not be definitively assigned due to significant overlap of ligand signals. ^{1}H NMR (600 MHz, C_6D_6): δ 2.41 – 2.33 (m, 4H), 2.33 – 2.25 (m, 4H), 2.14 – 2.02 (m, 6H), 1.93 – 1.77 (m, 15H), 1.77 – 1.69 (m, 4H), 1.61 – 1.49 (m, 6H), 1.48 – 1.23 (m, 14H), 1.23 – 1.12 (m, 3H), (d, 9H, J = 10.5 Hz, P-^{t}BuCH_3). ^{13}C {^{1}H} NMR (600 MHz, C_6D_6): δ 45.3 (t, J = 9.0 Hz), 44.9 (s), 36.3 (s), 35.1 (br s), 30.6 (s), 30.2 (s), 29.8 (s), 28.6 – 28.3 (m), 28.2 (br s), 27.2 (d, J = 29.2 Hz), 25.9 (dt, J = 13.2, 19.4 Hz), 25.6 (d, J = 4.6 Hz). ^{31}P {^{1}H} NMR (300 MHz, C_6D_6): 119.19 (t, 1P, J = 26.8 Hz), 86.99 (d, 2P, J = 27.2 Hz). δ IR (KBr): $\upsilon_{N\equiv N}$ = 2037 cm^{-1}. IR (C_5H_{12}): $\upsilon_{N\equiv N}$ = 2057 cm^{-1}.

Spectral Data for [^{t}BuP($CH_2CH_2P^iPr_2$)$_2$]Fe(C_2H_4) (3b). ^{1}H NMR (300 MHz, C_6D_6): δ 61.88 ($\upsilon_{1/2}$ = 286.6 Hz), 20.86 ($\upsilon_{1/2}$ = 235.5 Hz), 12.96 ($\upsilon_{1/2}$ = 150.9 Hz), 8.51 ($\upsilon_{1/2}$ = 108.9 Hz), -0.41 ($\upsilon_{1/2}$ = 114.5 Hz), -3.99 ($\upsilon_{1/2}$ = 165.4 Hz), -6.19 ($\upsilon_{1/2}$ = 186.3 Hz), -38.70 ($\upsilon_{1/2}$ = 174.0 Hz), -69.57 ($\upsilon_{1/2}$ = 207.1 Hz).

Spectral Data for [^{t}BuP($CH_2CH_2PCy_2$)$_2$]Fe(C_2H_4) (3c). ^{1}H NMR (600 MHz, C_6D_6): δ 47.80 ($\upsilon_{1/2}$ = 709.7 Hz), 19.64 ($\upsilon_{1/2}$ = 367.0 Hz), 15.77 ($\upsilon_{1/2}$ = 199.6 Hz), 12.59 ($\upsilon_{1/2}$ = 33.1 Hz), 7.48 ($\upsilon_{1/2}$ = 67.0 Hz), 5.65 ($\upsilon_{1/2}$ = 38.6 Hz), 4.03 ($\upsilon_{1/2}$ = 36.5 Hz), 3.06 ($\upsilon_{1/2}$ = 54.8 Hz), 0.14 ($\upsilon_{1/2}$ = 44.8 Hz), -0.05 ($\upsilon_{1/2}$ = 55.6 Hz), -2.16

($\upsilon_{1/2}$ = 876.6 Hz), -3.78 ($\upsilon_{1/2}$ = 198.2 Hz), -5.59 ($\upsilon_{1/2}$ = 417.4 Hz), -9.48 ($\upsilon_{1/2}$ = 386.1 Hz), -11.09 ($\upsilon_{1/2}$ = 678.3 Hz), -33.60 ($\upsilon_{1/2}$ = 391.3 Hz), -72.06 ($\upsilon_{1/2}$ = 396.4 Hz).

Spectral Data for [^{t}BuP($CH_2CH_2PEt_2$)$_2$]Fe(C_2H_4)$_2$ (4a). Selected ^{13}C {^{1}H} NMR (600 MHz, C_6D_6): δ 29.4 (m, H_2C=CH_2) and 24.7 (s, H_2C=CH_2). ^{31}P {^{1}H} NMR (300 MHz, C_6D_6): δ 156.74 (t, 1P, *J* = 16.6 Hz), 74.84 (d, 2P, *J* = 16.7 Hz).

Synthesis of [κ^2-^{t}BuP($CH_2CH_2P^iPr_2$)$_2$]Fe(η^6-C_6H_6) (5b). A 50 mL heavy walled glass reaction vessel was charged with 54 mg (0.11 mmol) **2b** and approximately 10 mL of C_6H_6. On a vacuum line, 1 atm $H_{2(g)}$ was admitted to the vessel at -196 °C. Immediately upon thawing, the solution turned from a light orange color to dark red. The reaction was stirred for 1 hour before removal of volatiles which yielded 53 mg (94% yield) of **5b** as a highly pentane soluble red oil. ^{1}H NMR (600 MHz, C_6D_6): δ 4.85 (s, 6H, C_6H_6), following signals assigned as P-C*H*, P-CH_2 and CH_3 of triphos ligand: 2.46 (m, 1H), 1.93 (m, 1H), 1.77 – 1.59 (m, 4H), 1.49 (m, 1H), 1.29 – 1.07 (m, 17H), 1.05 – 0.89 (m, 21H). ^{13}C {^{1}H} NMR (600 MHz, C_6D_6): δ 76.0 (s, C_6H_6), following signals assigned as P-*C*H, P-*C*H_2 and *C*H_3 of triphos ligand: 35.4 (d, *J* = 13.3 Hz), 29.3 (d, *J* = 13.5 Hz), 28.7 (d, *J* = 14.2 Hz), 28.2 (d, *J* = 4.0 Hz), 27.0 (dd, *J* = 6.8, 18.4 Hz), 24.6 (s), 24.5-24.3 (m), 24.0 (d, *J* = 14.6 Hz), 22.4 (dd, *J* = 18.8, 23.5 Hz), 20.6 (dd, *J* = 7.5, 16.4 Hz), 20.0 (d, *J* = 4.5 Hz), 19.5 (d, *J* = 2.0 Hz), 19.4 (s), 19.3 (s), 19.0 (s), 18.7 (br s), 18.5 (s), three resonances assumed to correspond to coincident carbons. ^{31}P {^{1}H} NMR (300 MHz, C_6D_6): δ 110.80 (d, 1P, *J* = 66.5 Hz), 109.61 (dd, 1P, *J* = 29.8, 66.2 Hz), 9.92 (d, 1P, *J* = 29.9 Hz).

Synthesis of [^{t}BuP($CH_2CH_2PEt_2$)$_2$]Fe(CO)$_2$ (6a). A 50 mL heavy walled glass reaction vessel was charged with 48 mg (0.11 mmol) of **1a,** 38 mg (0.28 mmol) KC_8, and approximately 10 mL THF inside a nitrogen filled glovebox. On a vacuum line, N_2 was removed from the reaction vessel via 2 freeze-pump-thaw cycles before addition of 1 atm CO at -196 °C. The reaction vessel was allowed to warm to ambient temperature and stirred overnight. The volatiles were then removed in vacuo, and the residue extracted with pentane.

The filtrate was slightly concentrated before recrystallizing at -35 °C overnight to afford 34 mg (74% yield) of **6a** as bright yellow crystals. Multiple NMR peaks could not be definitively assigned due to significant overlap of ligand signals. ^{1}H NMR (600 MHz, C_6D_6): δ 1.71 – 1.52 (m, 6H), 1.46 – 1.31 (m, 3H), 1.31 – 1.16 (m, 9H), 1.02 (d, 9H, *J* = 13.1 Hz), 0.94 – 0.82 (m, 10H). ^{13}C {^{1}H} NMR (600 MHz, C_6D_6): δ 232.8 (m, *C*≡O), 224.7 (m, *C*≡O), following signals assigned as P-*C*H$_2$ and *C*H$_3$ of triphos ligand: 33.1 (d, *J* = 20.4 Hz), 28.6 (ddd, *J* = 9.3, 12.4, 21.4 Hz), 27.1 (t, *J* = 12.7 Hz), 26.9 (d, *J* = 3.2 Hz), 25.9 (dt, *J* = 15.0, 19.8 Hz), 25.3 (t, *J* = 10.1 Hz), 8.7 (d, *J* = 29.6 Hz), one resonance assumed to correspond to coincident carbons. ^{31}P {^{1}H} NMR (300 MHz, C_6D_6): δ 163.23 (t, 1P, *J* = 54.5 Hz), 98.33 (d, 2P, *J* = 54.5 Hz). IR (KBr): $\upsilon_{C\equiv O}$ = 1827, 1880 cm^{-1}.

Synthesis of [^{t}BuP(CH$_2$CH$_2$P^{i}Pr$_2$)$_2$]Fe(CO)$_2$ (6b). This complex was prepared in a procedure analogous to that described for **6a**, using 62 mg (0.12 mmol) of **1b** and 43 mg (0.32 mmol) KC_8 to obtain 38 mg (63.3% yield) of **6b** as a yellow crystalline solid. Multiple NMR peaks could not be definitively assigned due to significant overlap of ligand signals. ^{1}H NMR (600 MHz, C_6D_6): δ 2.10 – 1.99 (m, 4H), 1.86 – 1.74 (m, 2H), 1.36 – 1.24 (m, 8H), 1.24 – 1.15 (m, 6H), 1.09 – 0.97 (m, 21H), 0.86 – 0.77 (m, 2H). ^{13}C {^{1}H} NMR (600 MHz, C_6D_6): δ 233.7 (dt, *J* = 25.2, 31.3 Hz, *C*≡O), 225.2 (dt, *J* = 11.3, 19.6 Hz, *C*≡O), following signals assigned as P-*C*H, P-*C*H$_2$ and *C*H$_3$ of triphos ligand: 34.4 (d, *J* = 19.6 Hz), 30.7 (t, *J* = 7.7 Hz), 30.3 (t, *J* = 11.8 Hz), 27.7 (dt, *J* = 14.3, 20.5 Hz), 27.5 (d, *J* = 3.5 Hz), 26.0 (ddd, *J* = 7.3, 10.6, 19.4 Hz), 19.5 (d, *J* = 27.6 Hz), 19.1 (d, *J* = 31.3 Hz). ^{31}P {^{1}H} NMR (300 MHz, C_6D_6): δ 160.77 (t, 1P, *J* = 48.2 Hz), 69.10 (d, 2P, *J* = 49.0 Hz). IR (KBr): $\upsilon_{C\equiv O}$ = 1834, 1890 cm^{-1}.

Synthesis of [^{t}BuP(CH$_2$CH$_2$PCy$_2$)$_2$]Fe(CO)$_2$ (6c). This complex was prepared in a procedure analogous to that described for **6a**, using 215 mg (0.32 mmol) of **1c** and 114 mg (0.84 mmol) KC_8 to obtain 116 mg (55.2% yield) of **6c** as a yellow crystalline solid. Multiple NMR peaks could not be definitively assigned due to significant overlap of ligand signals. ^{1}H NMR (600 MHz, C_6D_6): δ 2.21 (d, 2H, *J* = 12.6 Hz), 2.01 – 1.94 (m, 4H), 1.94 – 1.72 (m, 17H), 1.71 – 1.66 (m, 2H), 1.66 – 1.61 (m, 2H), 1.60 – 1.49 (m, 2H), 1.47 –

1.35 (m, 2H), 1.35 – 1.17 (m, 15H), 1.17 – 1.04 (m, 10H), 0.95 – 0.85 (m, 5H). ^{13}C {^{1}H} NMR (600 MHz, C_6D_6): δ 234.1 (dt, J = 25.9, 31.5 Hz, *C*≡O), 225.3 (dt, J = 11.3, 18.9 Hz, *C*≡O), following signals assigned as P-*C*H, P-*C*H_2 and *C*H_3 of triphos ligand: 41.5 – 41.1 (m), 34.3 (d, J = 19.4 Hz), 29.7 (s), 29.5 (d, J = 18.7 Hz), 28.6 (s), 28.2 (t, J = 5.1 Hz), 28.1 – 27.9 (m), 27.8 (t, J = 5.1 Hz), 27.6 (d, J = 3.3 Hz), 27.0 (d, J = 21.4 Hz), 25.4 (ddd, J = 7.3, 9.8, 19.0 Hz). ^{31}P {^{1}H} NMR (300 MHz, C_6D_6): δ 161.06 (t, 1P, J = 48.7 Hz), 110.84 (d, 2P, J = 48.1 Hz). IR (KBr): $\upsilon_{C\equiv O}$ = 1837, 1884 cm^{-1}.

General procedure for the quantification of CO_2 functionalization products. A J-Young style NMR tube was charged with 0.02 mmol of [^{t}BuP($CH_2CH_2PR_2$)$_2$]Fe(C_2H_4)(N_2) dissolved in C_6D_6. On a vacuum line, 0.12 mmol of C_2H_4 and 0.04 mmol of CO_2 were sequentially condensed into the tube at -196 °C. Upon thawing the sample, the reaction was allowed to proceed for 18 hours. During this time, all material crashed out of solution in the form of a lightly colored precipitate, and no NMR signals corresponding to a soluble organometallic species could be observed. Volatiles were then removed in vacuo, and the precipitate suspended in CD_3CN. The sample was next treated with 0.2 mmol of anhydrous HCl for approximately 15 minutes which caused all material to dissolve, forming a light-yellow solution. Following addition of a naphthalene internal integration standard, the yields of methylmalonic acid and propionic acid were calculated by quantitative ^{13}C NMR spectroscopy with a delay time of 60 seconds between transients.

Acknowledgements

This article is based upon work supported by the National Science Foundation (CHE-1955289) and the Curators of the Univ. of Missouri.

Associated Content

Supporting Information

The Supporting Information is available free of charge on the ACS Publications website at DOI: [to be inserted.]

Crystallographic Information Files (CCDC 2173057-2173060)

Selected NMR Spectra

Additional Experiment Descriptions

Competing Financial Interests

The authors declare no competing financial interests.

References

(1) Van Leeuwen, P. W. N. M.; Kamer, P. C. J.; Reek, J. N. H.; Dierkes, P. Ligand Bite Angle Effects in Metal-Catalyzed C−C Bond Formation. *Chem. Rev.* **2000**, *100* (8), 2741–2770. https://doi.org/10.1021/cr9902704.

(2) Pool, J. A.; Lobkovsky, E.; Chirik, P. J. Hydrogenation and Cleavage of Dinitrogen to Ammonia with a Zirconium Complex. *Nature* **2004**, *427* (6974), 527–530. https://doi.org/10.1038/nature02274.

(3) Khusnutdinova, J. R.; Milstein, D. Metal-Ligand Cooperation. *Angew. Chemie - Int. Ed.* **2015**, *54* (42), 12236–12273. https://doi.org/10.1002/anie.201503873.

(4) Zhang, Y.; MacIntosh, A. D.; Wong, J. L.; Bielinski, E. A.; Williard, P. G.; Mercado, B. Q.; Hazari, N.; Bernskoetter, W. H. Iron Catalyzed CO2 Hydrogenation to Formate Enhanced by Lewis Acid Co-Catalysts. *Chem. Sci.* **2015**, *6* (7), 4291–4299. https://doi.org/10.1039/c5sc01467k.

(5) Rønne, M. H.; Cho, D.; Madsen, M. R.; Jakobsen, J. B.; Eom, S.; Escoudé, É.; Hammershøj, H. C. D.; Nielsen, D. U.; Pedersen, S. U.; Baik, M. H.; Skrydstrup, T.; Daasbjerg, K. Ligand-Controlled Product Selectivity in Electrochemical Carbon Dioxide Reduction Using Manganese Bipyridine Catalysts. *J. Am. Chem. Soc.* **2020**, *142* (9), 4265–4275. https://doi.org/10.1021/jacs.9b11806.

(6) Manriquez, J. M.; Bercaw, J. E. Preparation of a Dinitrogen Complex of Bis(Pentamethylcyclopentadienyl)Zirconium(II). Isolation and Protonation Leading to Stoichiometric Reduction of Dinitrogen to Hydrazine. *J. Am. Chem. Soc.* **1974**, *96* (19), 6229–6230. https://doi.org/10.1021/ja00826a071.

(7) Laitar, D. S.; Müller, P.; Sadighi, J. P. Efficient Homogeneous Catalysis in the Reduction of CO2 to CO. *J. Am. Chem. Soc.* **2005**, *127* (49), 17196–17197. https://doi.org/10.1021/ja0566679.

(8) Costentin, C.; Passard, G.; Robert, M.; Savéant, J. M. Ultraefficient Homogeneous Catalyst for the CO2-to-CO Electrochemical Conversion. *Proc. Natl. Acad. Sci. U. S. A.* **2014**, *111* (42), 14990–14994. https://doi.org/10.1073/pnas.1416697111.

(9) Ouyang, T.; Wang, H. J.; Huang, H. H.; Wang, J. W.; Guo, S.; Liu, W. J.; Zhong, D. C.; Lu, T. B. Dinuclear Metal Synergistic Catalysis Boosts Photochemical CO2-to-CO Conversion. *Angew. Chemie - Int. Ed.* **2018**, *57* (50), 16480–16485. https://doi.org/10.1002/anie.201811010.

(10) Tanaka, R.; Yamashita, M.; Nozaki, K. Catalytic Hydrogenation of Carbon Dioxide Using Ir(III)-Pincer Complexes. *J. Am. Chem. Soc.* **2009**, *131* (40), 14168–14169. https://doi.org/10.1021/ja903574e.

(11) Zhang, Y.; MacIntosh, A. D.; Wong, J. L.; Bielinski, E. A.; Williard, P. G.; Mercado, B. Q.; Hazari, N.; Bernskoetter, W. H. Iron Catalyzed CO2 Hydrogenation to Formate Enhanced by Lewis Acid Co-Catalysts. *Chem. Sci.* **2015**, *6* (7), 4291–4299. https://doi.org/10.1039/c5sc01467k.

(12) Schieweck, B. G.; Westhues, N. F.; Klankermayer, J. A Highly Active Non-Precious Transition Metal Catalyst for the Hydrogenation of Carbon Dioxide to Formates. *Chem. Sci.* **2019**, *10* (26), 6519–6523. https://doi.org/10.1039/c8sc05230a.

(13) Chen, B.; Dong, M.; Liu, S.; Xie, Z.; Yang, J.; Li, S.; Wang, Y.; Du, J.; Liu, H.; Han, B. CO2Hydrogenation to Formate Catalyzed by Ru Coordinated with a N,P-Containing Polymer. *ACS Catal.* **2020**, *10* (15), 8557–8566. https://doi.org/10.1021/acscatal.0c01678.

(14) Kar, S.; Kothandaraman, J.; Goeppert, A.; Prakash, G. K. S. Advances in Catalytic Homogeneous Hydrogenation of Carbon Dioxide to Methanol. *J. CO2 Util.* **2018**, *23* (December 2017), 212–218. https://doi.org/10.1016/j.jcou.2017.10.023.

(15) Zhong, J.; Yang, X.; Wu, Z.; Liang, B.; Huang, Y.; Zhang, T. State of the Art and Perspectives in Heterogeneous Catalysis of CO2 Hydrogenation to Methanol. *Chem. Soc. Rev.* **2020**, *49* (5), 1385–1413. https://doi.org/10.1039/c9cs00614a.

(16) Tominaga, K.; Sasaki, Y.; Watanabe, T.; Saito, M. Homogeneous Hydrogenation of Carbon Dioxide to Methanol Catalyzed by Ruthenium Cluster Anions in the Presence of Halide Anions. *Bull. Chem. Soc. Jpn.* **1995**, *68* (10), 2837–2842. https://doi.org/10.1246/bcsj.68.2837.

(17) Schneidewind, J.; Adam, R.; Baumann, W.; Jackstell, R.; Beller, M. Low-Temperature Hydrogenation of Carbon Dioxide to Methanol with a Homogeneous Cobalt Catalyst. *Angew. Chemie - Int. Ed.* **2017**, *56* (7), 1890–1893. https://doi.org/10.1002/anie.201609077.

(18) Zubar, V.; Lebedev, Y.; Azofra, L. M.; Cavallo, L.; El-Sepelgy, O.; Rueping, M. Hydrogenation of CO2-Derived Carbonates and Polycarbonates to Methanol and Diols by Metal–Ligand Cooperative Manganese Catalysis. *Angew. Chemie - Int. Ed.* **2018**, *57* (41), 13439–13443. https://doi.org/10.1002/anie.201805630.

(19) Kar, S.; Sen, R.; Kothandaraman, J.; Goeppert, A.; Chowdhury, R.; Munoz, S. B.; Haiges, R.; Prakash, G. K. S. Mechanistic Insights into Ruthenium-Pincer-Catalyzed Amine-Assisted Homogeneous Hydrogenation of CO 2 to Methanol. *J. Am. Chem. Soc.* **2019**, *141* (7), 3160–3170. https://doi.org/10.1021/jacs.8b12763.

(20) Wang, X.; Wang, H.; Sun, Y. Synthesis of Acrylic Acid Derivatives from CO2 and Ethylene. *Chem* **2017**, *3* (2), 211–228. https://doi.org/10.1016/j.chempr.2017.07.006.

(21) Hoberg, H.; Schaefer, D. Nickel(0) Induzierte C-C Verknupfung Zwischen Alkenen Und Kohlendioxid. *J. Organomet. Chem.* **1982**, *236* (1982), C28–C30.

(22) Lejkowski, M. L.; Lindner, R.; Kageyama, T.; Bódizs, G. É.; Plessow, P. N.; Müller, I. B.; Schäfer, A.; Rominger, F.; Hofmann, P.; Futter, C.; Schunk, S. A.; Limbach, M. The First

Catalytic Synthesis of an Acrylate from CO2 and an Alkene-A Rational Approach. *Chem. - A Eur. J.* **2012**, *18* (44), 14017–14025. https://doi.org/10.1002/chem.201201757.

(23) Hopkins, M. N.; Shimmei, K.; Uttley, K. B.; Bernskoetter, W. H. Synthesis and Reactivity of 1,2-Bis(Di- Iso-Propylphosphino)Benzene Nickel Complexes: A Study of Catalytic CO 2 -Ethylene Coupling. *Organometallics* **2018**, *37* (20), 3573–3580. https://doi.org/10.1021/acs.organomet.8b00260.

(24) Takahashi, K.; Cho, K.; Iwai, A.; Ito, T.; Iwasawa, N. Development of N-Phosphinomethyl-Substituted NHC-Nickel(0) Complexes as Robust Catalysts for Acrylate Salt Synthesis from Ethylene and CO2. *Chem. - A Eur. J.* **2019**, *25* (59), 13504–13508. https://doi.org/10.1002/chem.201903625.

(25) Ito, T.; Takahashi, K.; Iwasawa, N. Reactivity of a Ruthenium(0) Complex Bearing a Tetradentate Phosphine Ligand: Applications to Catalytic Acrylate Salt Synthesis from Ethylene and CO2. *Organometallics* **2019**, *38* (2), 205–209. https://doi.org/10.1021/acs.organomet.8b00789.

(26) Takahashi, K.; Hirataka, Y.; Ito, T.; Iwasawa, N. Mechanistic Investigations of the Ruthenium-Catalyzed Synthesis of Acrylate Salt from Ethylene and CO 2. *Organometallics* **2020**, *39* (9), 1561–1572. https://doi.org/10.1021/acs.organomet.9b00659.

(27) Uttley, K. B.; Shimmei, K.; Bernskoetter, W. H. Ancillary Ligand and Base Influences on Nickel-Catalyzed Coupling of CO2 and Ethylene to Acrylate. *Organometallics* **2020**, *39*, 1573–1579. https://doi.org/10.1021/acs.organomet.9b00708.

(28) Adamson, T. T.; Kelley, S. P.; Bernskoetter, W. H. Iron-Mediated C–C Bond Formation via Reductive Coupling with Carbon Dioxide. *Organometallics* **2020**, *39* (19), 3562–3571. https://doi.org/10.1021/acs.organomet.0c00528.

(29) Takahashi, K.; Sakurazawa, Y.; Iwai, A.; Iwasawa, N. Catalytic Synthesis of a Methylmalonate

Salt from Ethylene and Carbon Dioxide through Photoinduced Activation and Photoredox-Catalyzed Reduction of Nickelalactones. *ACS Catal.* **2022**, *12* (7), 3776–3781. https://doi.org/10.1021/acscatal.2c01053.

(30) Aresta, M.; Pastore, C.; Giannoccaro, P.; Kovács, G.; Dibenedetto, A.; Pápai, I. Evidence for Spontaneous Release of Acrylates from a Transition-Metal Complex upon Coupling Ethene or Propene with a Carboxylic Moiety or CO 2. *Chem. - A Eur. J.* **2007**, *13* (32), 9028–9034. https://doi.org/10.1002/chem.200700532.

(31) Greenburg, Z. R.; Jin, D.; Williard, P. G.; Bernskoetter, W. H. Nickel Promoted Functionalization of CO2 to Anhydrides and Ketoacids. *Dalt. Trans.* **2014**, *43* (42), 15990–15996. https://doi.org/10.1039/c4dt01221f.

(32) Yu, B.; Diao, Z. F.; Guo, C. X.; He, L. N. Carboxylation of Olefins/Alkynes with CO2to Industrially Relevant Acrylic Acid Derivatives. *J. CO2 Util.* **2013**, *1* (February 2021), 60–68. https://doi.org/10.1016/j.jcou.2013.01.001.

(33) Inoue, Y.; Itoh, Y.; Hashimoto, H. Incorporation of Carbon Dioxide in Alkyne Oligomerization Catalyzed By Nickel(0) Complexes. Formation of Substituted 2-Pyrones. *Chem. Lett.* **1977**, *6* (8), 855–856. https://doi.org/10.1246/cl.1977.855.

(34) Yasuo Fukue, Shinichi Oi, Y. I. Direct Synthesis of Alkyl2-Alkynoates from Alk-l-Ynes, C02, and Bromoalkanes Catalysed by Copper(1) or Silver(1) Salt. *J. Chem. Soc., Chem. Commun.* **1994**, No. 18, 2091.

(35) Yu, D.; Zhang, Y. Copper- and Copper– N -Heterocyclic Carbene-Catalyzed C─H Activating Carboxylation of Terminal Alkynes with CO 2 at Ambient Conditions. *Proc. Natl. Acad. Sci.* **2010**, *107* (47), 20184–20189. https://doi.org/10.1073/pnas.1010962107.

(36) Zhang, X.; Zhang, W. Z.; Ren, X.; Zhang, L. L.; Lu, X. B. Ligand-Free Ag(I)-Catalyzed

Carboxylation of Terminal Alkynes with CO 2. *Org. Lett.* **2011**, *13* (9), 2402–2405. https://doi.org/10.1021/ol200638z.

(37) Yuan, R.; Lin, Z. Mechanism for the Carboxylative Coupling Reaction of a Terminal Alkyne, CO2, and an Allylic Chloride Catalyzed by the Cu(I) Complex: A DFT Study. *ACS Catal.* **2014**, *4* (12), 4466–4473. https://doi.org/10.1021/cs5011184.

(38) Wang, X.; Nakajima, M.; Martin, R. Ni-Catalyzed Regioselective Hydrocarboxylation of Alkynes with CO2 by Using Simple Alcohols as Proton Sources. *J. Am. Chem. Soc.* **2015**, *137* (28), 8924–8927. https://doi.org/10.1021/jacs.5b05513.

(39) Jurd, P. M.; Li, H. L.; Bhadbhade, M.; Dalgarno, S. J.; McIntosh, R. D.; Field, L. D. The Reaction of Iron Acetylides with Carbon Dioxide. *Organometallics* **2020**, *39* (9), 1580–1589. https://doi.org/10.1021/acs.organomet.9b00830.

(40) Jurd, P. M.; Li, H. L.; Bhadbhade, M.; Watson, J. D.; Field, L. D. Ferralactone Formation from Iron Acetylides and Carbon Dioxide. *J. Organomet. Chem.* **2022**, *961*, 122252. https://doi.org/10.1016/j.jorganchem.2021.122252.

(41) Burkart, M. D.; Hazari, N.; Tway, C. L.; Zeitler, E. L. Opportunities and Challenges for Catalysis in Carbon Dioxide Utilization. *ACS Catal.* **2019**, *9* (9), 7937–7956. https://doi.org/10.1021/acscatal.9b02113.

(42) Hoberg, H.; Jenni, K.; Krüger, C.; Raabe, E. CC-Kupplung von CO2 Und Butadien an Eisen(o)-Komplexen – Ein Neuer Weg Zu α,ω-Dicarbonsäuren. *Angew. Chemie* **1986**, *98* (9), 819–820. https://doi.org/10.1002/ange.19860980915.

(43) Davis, I. S. R. E.; Sot, J. A. C.; Steudel, R.; Maude, H.; Hoberg, B. H.; Jenni, K.; Angermund, K. CC-Linkages of Ethene with CO2, on an Iron(o) Complex-Synthesis and Crystal Structure Analysis of I(PEt3)2Fe(C2H4)21. *Angew Chem. Inr Ed. Engl* **1987**, *93* (1981), 153–155.

(44) Gibson, D. H. The Organometallic Chemistry of Carbon Dioxide. *Chem. Rev.* **1996**, *96* (6), 2063–2095. https://doi.org/10.1021/cr940212c.

(45) Blum, O.; Milstein, D. Mechanism of a Directly Observed β-Hydride Elimination Process of Iridium Alkoxo Complexes. *J. Am. Chem. Soc.* **1995**, *117* (16), 4582–4594. https://doi.org/10.1021/ja00121a016.

(46) Glascoe, E. A.; Kling, M. F.; Shanoski, J. E.; DiStasio, R. A.; Payne, C. K.; Mork, B. V.; Don Tilley, T.; Harris, C. B. Photoinduced β-Hydrogen Elimination and Radical Formation with CpW(CO)3(CH2CH3): Ultrafast IR and DFT Studies. *Organometallics* **2007**, *26* (6), 1424–1432. https://doi.org/10.1021/om060455i.

(47) DuBois, D. L.; Miedaner, A.; Haltiwanger, R. C. Electrochemical Reduction of CO2 Catalyzed by [Pd(Triphosphine)(Solvent)](BF4)2 Complexes: Synthetic and Mechanistic Studies. *J. Am. Chem. Soc.* **1991**, *113* (23), 8753–8764. https://doi.org/10.1021/ja00023a023.

(48) Liao, Q.; Saffon-Merceron, N.; Mézailles, N. N2 Reduction into Silylamine at Tridentate Phosphine/Mo Center: Catalysis and Mechanistic Study. *ACS Catal.* **2015**, *5* (11), 6902–6906. https://doi.org/10.1021/acscatal.5b01626.

(49) Cavaillé, A.; Joyeux, B.; Saffon-Merceron, N.; Nebra, N.; Fustier-Boutignon, M.; Mézailles, N. Triphos-Fe Dinitrogen and Dinitrogen-Hydride Complexes: Relevance to Catalytic N2 Reduction. *Chem. Commun.* **2018**, *54* (84), 11953–11956. https://doi.org/10.1039/c8cc07466f.

(50) Evans, D. F. 400. The Determination of the Paramagnetic Susceptibility of Substances in Solution by Nuclear Magnetic Resonance. *J. Chem. Soc.* **1959**, 2003–2005. https://doi.org/10.1039/jr9590002003.

(51) Knopf, I.; Tofan, D.; Beetstra, D.; Al-Nezari, A.; Al-Bahily, K.; Cummins, C. C. A Family of Cis-Macrocyclic Diphosphines: Modular, Stereoselective Synthesis and Application in Catalytic

CO2/Ethylene Coupling. *Chem. Sci.* **2017**, *8* (2), 1463–1468. https://doi.org/10.1039/c6sc03614g.

(52) Vavasori, A.; Calgaro, L.; Pietrobon, L.; Ronchin, L. The Coupling of Carbon Dioxide with Ethene to Produce Acrylic Acid Sodium Salt in One Pot by Using Ni(II) and Pd(II)-Phosphine Complexes as Precatalysts. *Pure Appl. Chem.* **2018**, *90* (2), 315–326. https://doi.org/10.1515/pac-2017-0706.

(53) Kim, J.; Hahm, H.; Ryu, J. Y.; Byun, S.; Park, D. A.; Lee, S. H.; Lim, H.; Lee, J.; Hong, S. Pyridine-Chelated Imidazo[1,5-a]Pyridine n-Heterocyclic Carbene Nickel(II) Complexes for Acrylate Synthesis from Ethylene and Co2. *Catalysts* **2020**, *10* (7). https://doi.org/10.3390/catal10070758.

(54) Jin, D.; Schmeier, T. J.; Williard, P. G.; Hazari, N.; Bernskoetter, W. H. Lewis Acid Induced β-Elimination from a Nickelalactone: Efforts toward Acrylate Production from CO2 and Ethylene. *Organometallics* **2013**, *32* (7), 2152–2159. https://doi.org/10.1021/om400025h.

(55) Stieber, S. C. E.; Huguet, N.; Kageyama, T.; Jevtovikj, I.; Ariyananda, P.; Gordillo, A.; Schunk, S. A.; Rominger, F.; Hofmann, P.; Limbach, M. Acrylate Formation from CO2 and Ethylene: Catalysis with Palladium and Mechanistic Insight. *Chem. Commun.* **2015**, *51* (54), 10907–10909. https://doi.org/10.1039/c5cc01932j.

(56) Manzini, S.; Cadu, A.; Schmidt, A.-C.; Huguet, N.; Trapp, O.; Paciello, R.; Schaub, T. Enhanced Activity and Recyclability of Palladium Complexes in the Catalytic Synthesis of Sodium Acrylate from Carbon Dioxide and Ethylene. *ChemCatChem* **2017**, *9* (12), 2269–2274. https://doi.org/10.1002/cctc.201601150.

(57) Rummelt, S. M.; Zhong, H.; Korobkov, I.; Chirik, P. J. Iron-Mediated Coupling of Carbon Dioxide and Ethylene: Macrocyclic Metallalactones Enable Access to Various Carboxylates. *J. Am. Chem. Soc.* **2018**, *140* (37), 11589–11593. https://doi.org/10.1021/jacs.8b07558.

(58) Michel, J. A.; Robinson, V. S.; Yang, L.; Sambandam, S.; Lu, W.; Westover, T.; Fisher, T. S.; Lukehart, C. M. Synthesis and Characterization of Potassium Metal/Graphitic Carbon Nanofiber Intercalates. *J. Nanosci. Nanotechnol.* **2008**, *8* (4), 1942–1950. https://doi.org/10.1166/jnn.2008.308.

(59) Addison, A. W.; Rao, T. N.; Reedijk, J.; van Rijn, J.; Verschoor, G. C. Synthesis, Structure, and Spectroscopic Properties of Copper(II) Compounds Containing Nitrogen–Sulphur Donor Ligands; the Crystal and Molecular Structure of Aqua[1,7-Bis(N-Methylbenzimidazol-2′-Yl)-2,6-Dithiaheptane]Copper(II) Perchlorate. *J. Chem. Soc., Dalt. Trans.* **1984**, No. 7, 1349–1356. https://doi.org/10.1039/DT9840001349.

(60) Blackman, A. G.; Schenk, E. B.; Jelley, R. E.; Krenske, E. H.; Gahan, L. R. Five-Coordinate Transition Metal Complexes and the Value of τ 5 : Observations and Caveats. *Dalt. Trans.* **2020**, *49* (42), 14798–14806. https://doi.org/10.1039/D0DT02985H.

(61) Ryther, R. J.; Weitz, E. Reaction Kinetics of Coordinatively Unsaturated Iron Carbonyls Formed on Gas-Phase Excimer Laser Photolysis of Fe(CO)5. *J. Phys. Chem.* **1991**, *95* (24), 9841–9852. https://doi.org/10.1021/j100177a043.

(62) Harvey, J. N.; Poli, R. Computational Study of the Spin-Forbidden H2 Oxidative Addition to 16-Electron Fe(0) Complexes. *J. Chem. Soc. Dalt. Trans.* **2003**, *3* (21), 4100–4106. https://doi.org/10.1039/b302916f.

(63) Casitas, A.; Krause, H.; Goddard, R.; Fürstner, A. Elementary Steps of Iron Catalysis: Exploring the Links between Iron Alkyl and Iron Olefin Complexes for Their Relevance in C-H Activation and C-C Bond Formation. *Angew. Chemie - Int. Ed.* **2015**, *54* (5), 1521–1526. https://doi.org/10.1002/anie.201410069.

(64) ^{31}P NMR (300 MHz, C_6D_6) data for free ^{t}BuP($CH_2CH_2P^{i}Pr_2$)$_2$: δ 9.83 – 9.02 (m).

(65) Howarth, L.; Wong, L. L. Substitution Reactions of the Zerovalent Iron Complexes [Fe(η-C6H6)(PMe3)2] and [Fe(η-C6H6)(Dmpe)] (Dmpe = Me2PCH2CH2PMe2). *J. Chem. Soc. Dalt. Trans.* **1989**, No. 7, 1385–1391. https://doi.org/10.1039/DT9890001385.

(66) See the Experimental Section and the Supporting Information for details.

(67) Falivene, L.; Cao, Z.; Petta, A.; Serra, L.; Poater, A.; Oliva, R.; Scarano, V.; Cavallo, L. Towards the Online Computer-Aided Design of Catalytic Pockets. *Nat. Chem.* **2019**, *11* (10), 872–879. https://doi.org/10.1038/s41557-019-0319-5.

(68) Jurd, P. M.; Li, H. L.; Bhadbhade, M.; Field, L. D. Fe(0)-Mediated Reductive Disproportionation of CO 2. *Organometallics* **2020**, *39*, 2011–2018. https://doi.org/10.1021/acs.organomet.0c00175.

(69) Palacios, E. G.; Juárez-López, G.; Monhemius, A. J. Infrared Spectroscopy of Metal Carboxylates: II. Analysis of Fe(III), Ni and Zn Carboxylate Solutions. *Hydrometallurgy* **2004**, *72* (1–2), 139–148. https://doi.org/10.1016/S0304-386X(03)00137-3.

(70) Yost, E. C.; Tejedor-Tejedor, M. I.; Anderson, M. A. In Situ CIR-FTIR Characterization off Salicylate Complexes at the Goethite/Aqueous Solution Interface. *Environ. Sci. Technol.* **1990**, *24* (6), 822–828. https://doi.org/10.1021/es00076a005.

(71) Jin, D.; Williard, P. G.; Hazari, N.; Bernskoetter, W. H. Effect of Sodium Cation on Metallacycle β-Hydride Elimination in CO2-Ethylene Coupling to Acrylates. *Chem. - A Eur. J.* **2014**, *20* (11), 3205–3211. https://doi.org/10.1002/chem.201304196.

(72) Allen, O. R.; Dalgarno, S. J.; Field, L. D.; Jensen, P.; Turnbull, A. J.; Willis, A. C. Addition of CO2 to Alkyl Iron Complexes, Fe(PP) 2Me2. *Organometallics* **2008**, *27* (9), 2092–2098. https://doi.org/10.1021/om800091a.

(73) Pangborn, A. B.; Giardello, M. A.; Grubbs, R. H.; Rosen, R. K.; Timmers, F. J. Safe and Convenient Procedure for Solvent Purification. *Organometallics* **1996**, *15* (5), 1518–1520.

https://doi.org/10.1021/om9503712.

(74) Fulmer, G. R.; Miller, A. J. M.; Sherden, N. H.; Gottlieb, H. E.; Nudelman, A.; Stoltz, B. M.; Bercaw, J. E.; Goldberg, K. I. NMR Chemical Shifts of Trace Impurities: Common Laboratory Solvents, Organics, and Gases in Deuterated Solvents Relevant to the Organometallic Chemist. *Organometallics* **2010**, *29* (9), 2176–2179. https://doi.org/10.1021/om100106e.

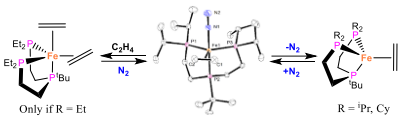
Et2P
Fe
Et2P
P tBu
C2H4
N2
-N2
+N2
R2P
R2P
Fe
P tBu
Only if R = Et
R = iPr, Cy

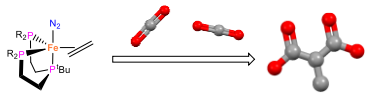
N2
R2P
R2P
Fe
P tBu